arXiv:1609.00540v2 [cond-mat.soft] 15 Nov 2016

Interplay between adsorption and hydrodynamics in nanochannels: towards tunable membranes

Sela Samin* and René van Roij
Institute for Theoretical Physics, Center for Extreme Matter and Emergent Phenomena, Utrecht University, Princetonplein 5, 3584 CC Utrecht, The Netherlands
(Dated: November 16, 2016)

We study how adsorption of a near-critical binary mixture in a nanopore is modified by flow inside the pore. We identify three types of steady states upon variation of the pore Péclet number (Pe_p), which can be reversibly accessed by the application of an external pressure. Interestingly, for small Pe_p the pore acts as a weakly selective membrane which separates the mixture. For intermediate Pe_p, the flow effectively shifts the adsorption in the pore thereby opening possibilities for enhanced and tunable solute transport through the pore. For large Pe_p, the adsorption is progressively reduced inside the pore, accompanied by a long ranged dispersion of the mixture far from the pore.

Pressure-driven membrane processes are widely used in water treatment technology [1]. With the aim of producing more energy-efficient and eco-friendly membranes, intense ongoing research is dedicated to the improvement of the membrane's conductivity and selectivity [2–4] and to prevent fouling [5]. Yet, advances are impeded by the lacking understanding of transport in membranes used for removing various organic contaminants or oil spills from water [6], in pressure-driven hydrocarbon recovery in nanoporous rocks [7, 8], and organic solvent nanofiltration [9–11].

Also from a fundamental perspective, the role of hydrodynamics in phase separation kinetics [12] near wetting surfaces [13] and in confinement [14, 15] has been extensively studied, as well as its role in wetting of immiscible oil-water systems in micro- and nano-channels [16], and in nanobubbles formation [17]. More recently, capillary driven flows in nanometric channels have been extensively studied [18, 19], also in mixtures [20].

The consequences of pressure-induced flow across a nano-channel and perpendicular to a wetting or adsorption layer have been studied before in the context of electrolyte [21–23] and polymer [24] solutions. However, the consequences for a non-ideal liquid mixture, where the hydrodynamics-adsorption coupling of the solvent itself is temperature- and composition-sensitive, has not been explored before to the best of our knowledge. This scenario is, however, common in *any* membrane process involving liquid mixtures and also bears resemblance to the classical Graetz problem of mass (or heat) transfer into a fluid in steady flow through a cylindrical tube [25, 26]. Nevertheless, there are important differences. Unlike the Graetz problem, there is no net flux of material from a wetting wall into the fluid. More importantly, when the adsorbed fluid is the solvent itself, in contrast to the dilute gas typically considered in the Graetz problem and general mass transfer problems, an important length scale appears, namely, the correlation length ξ. In this Letter, we show that when ξ is of the order of the channel size, hydrodynamics and wetting become strongly coupled, leading to several surprising effects. We focus on the critical adsorption regime [27], in the one-phase regime close to the critical temperature T_c of the mixture, where ξ is naturally large. However, our results should be applicable whenever the thickness of the adsorbed film is comparable to the channel size, also far from T_c.

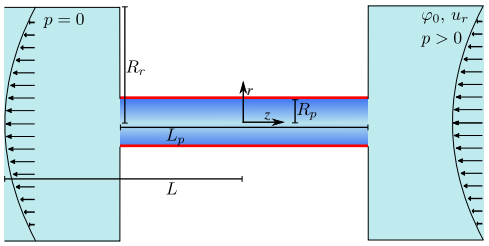

FIG. 1. Schematic illustration of a cylindrical pore with radius R_p and length L_p connecting two reservoirs with radius R_r and length $L - L_p/2$. In equilibrium, the reservoirs' compositions are φ_0 but inside the pore the composition is larger due to solvent adsorption to the attractive pore wall (red line). After the application of pressure to the right reservoir, a Hagen–Poiseuille flow with a parabolic velocity profile and an average velocity u_r develops far from the pore.

Using Direct Numerical Simulations (DNS) we explore the effect of solvent adsorption to channel walls in nanofluidic systems of binary mixtures. We consider a near-critical binary mixture characterized by the order parameter φ, which denotes the deviation of the mixture volume fraction from its critical value φ_c. By near-critical we mean that the mixture temperature T and average composition φ_0 are in the neighborhood of the critical point (T_c, φ_c). Two cylindrical material reservoirs with radius R_r and length $L - L_p/2$ containing the mixture are connected by a narrow cylindrical pore with radius R_p and length L_p, see Fig. 1. In equilibrium, the composition of both reservoirs is φ_0 but inside the pore $\varphi > \varphi_0$ is not uniform since the pore wall favors one component. Close enough to T_c the mixture correlation length ξ becomes comparable to R_p and $\varphi > \varphi_0$ throughout the pore volume [28, 29] due to adsorption. We then impose a pressure at the edge of right reservoir in Fig. 1,

forcing the mixture through the pore and leading to a fully-developed Hagen–Poiseuille flow with a mean velocity u_r far from the pore. For an incompressible fluid, the mean velocity in the pore is hence $u_p = (R_r/R_p)^2 u_r$.

To investigate the dynamics and steady-state we employ a classical continuum framework [30]. The time evolution of the fluid is given by the so-called model-H equations, combining the convective Cahn-Hilliard equation for the composition with the Stokes equations for the fluid velocity for small Reynolds number, $\mathrm{Re} \ll 1$. In dimensionless form the governing equations read

$$\partial\varphi/\partial t = -\nabla\cdot(\mathrm{Pe}_p\varphi\boldsymbol{v} - \nabla\mu) \ , \tag{1}$$

$$\mu = -\epsilon\nabla^2\varphi + f'(\varphi) \ , \tag{2}$$

$$\nabla\cdot\boldsymbol{v} = 0 \ , \tag{3}$$

$$\nabla\cdot\boldsymbol{\tau} = \nabla p + {\mathrm{C_h}}^{-1}\mathrm{Ca}^{-1}\varphi\nabla\mu \ . \tag{4}$$

Here, all lengths are scaled by R_p, the velocity $\boldsymbol{v}$ by u_p, the chemical potential μ by the thermal energy k_BT, and time is scaled by R_p^2/D, where D is the mixture inter-diffusion constant. Three dimensionless groups appear in this form of the equations. The most important is the Péclet number in the pore, $\mathrm{Pe}_p = u_pR_p/D$, measuring the relative magnitude of the composition advective current, $\boldsymbol{j_a} = \mathrm{Pe}_p\varphi\boldsymbol{v}$, and diffusive current, $\boldsymbol{j_d} = -\nabla\mu$, in Eq. (1). The chemical potential is derived from a Ginzburg-Landau free-energy for a LCST-type mixture [31], where the Laplacian term in Eq. (2) accounts for composition inhomogeneities and the bulk part is given by the derivative of $f = \alpha\varphi^2/2 + 4\varphi^4/3$, where $\alpha = 2(\chi - 2)$ with $\chi \sim 1/T$ the Flory interaction parameter. Composition gradients are characterized by $\epsilon = \chi{\mathrm{C_h}}^2$ [32], where $\mathrm{C_h} = a/R_p$ is the Cahn number, with a a molecular length characterizing both mixture components. In the Stokes equations, Eqs. (3) and (4), p and $\boldsymbol{\tau} = \nabla\boldsymbol{v} + \nabla\boldsymbol{v}^T$ are the dimensionless fluid pressure and viscous stress tensor, respectively, scaled by $\eta u_p/R_p$, where η is the fluid viscosity. The last term in (4) is a body force due to chemical potential gradients, which is inversely proportional to the capillary number, $\mathrm{Ca} = a^2\eta u_p/k_BT$, measuring the relative magnitude of viscous and interfacial forces.

We use a cylindrical system of coordinates (r, z) with $z \in [-L, L]$ and $r \in [0, R_r]$, and employ symmetry boundary conditions (BCs) at $r = 0$. At the inlet ($z = L$) we impose a critical composition with $\varphi_0 = \varphi_c = 0$, the corresponding chemical potential $\mu_0 = 0$ and a fully-developed laminar flow with a mean velocity u_r (see Fig. 1). At the outlet ($z = -L$), we allow the mixture to be freely advected [31]. On all other solid boundaries we impose no-slip for the velocity $\boldsymbol{v} = 0$ [33] and no composition flux, $\boldsymbol{n}\cdot\nabla\mu = 0$, where $\boldsymbol{n}$ is the outward unit vector normal to the surface. At the reservoir walls $\boldsymbol{n}\cdot\nabla\varphi = 0$, as there is no adsorption of either component. The pore wall, however, does preferentially adsorb one of the components, and therefore $\boldsymbol{n}\cdot\nabla\varphi|_{r=R_p} = \gamma/\epsilon$ for $|z| < L_p/2$,

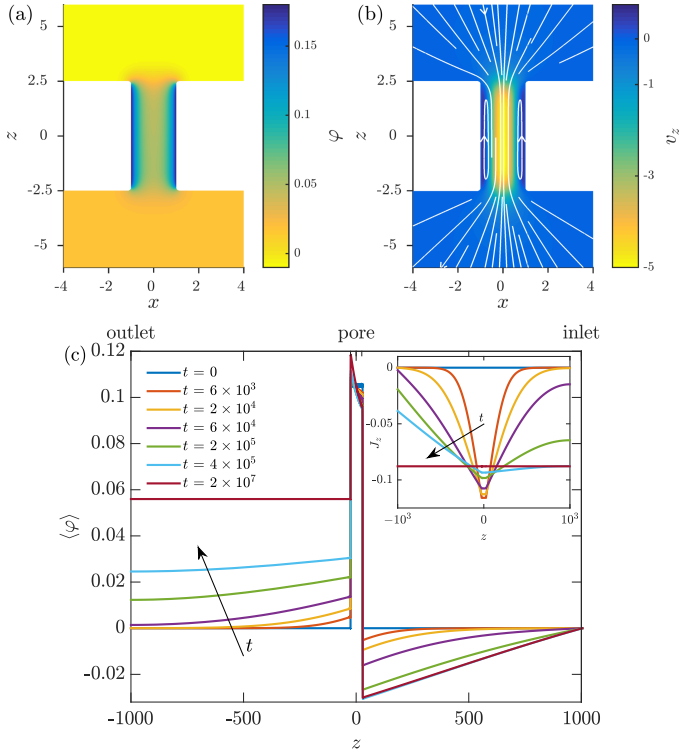

FIG. 2. (color online) (a) composition and (b) velocity z-component and streamlines for steady state case (i) in the xOz plane for a mixture at a temperature $T_c - 3$ K ($\xi = 4.86$ nm) and with $u_p = 0.05$ mm/s ($\mathrm{Pe}_p = 0.0077$). The unit of length in all figures is the pore radius $R_p = 5$ nm, and here we also set $L_p = 5$, $R_r = 20$ and $L = 10^3$, i.e., the reservoirs' edges and their side walls are (far) beyond the scale of this plot. (c) Time evolution of the radially averaged composition $\langle\varphi\rangle$ profiles for case (i) using same the parameters as in (a) but with $L_p = 50$. Inset: the corresponding z-component of the composition current $\boldsymbol{J}_z$ (see text).

where γ measures the difference between the short-range interaction of the two solvent components and the solid [34]. We use $\gamma = 0.1\mathrm{C_h}$ that leads to weak critical adsorption [35].

For concreteness, we use the physical properties of the experimentally common mixture water–2,6-lutidine [31, 36]. Using typical values leads to $\mathrm{Ca} \sim 10^{-6} - 10^{-4}$ and $\mathrm{C_h} \sim 0.1 - 0.01$ for pore mean velocities $u_p \sim 0.1 - 10$ mm/s and pore radii $R_p \sim 1 - 10$ nm. Unlike other properties, the inter-diffusion constant is sensitive to temperature, and close to T_c it follows the Stokes-Einstein-Kawasaki-Ferrell relation [37] $D = k_BT/(6\pi\eta\xi)$, where the correlation length ξ in our mean-field description follows the scaling $\xi \propto (|T - T_c|/T)^{-1/2}$ [38]. Hence, for u_p mentioned above and for $T - T_c \sim 1 - 10$ K we find $\mathrm{Pe}_p \sim 0.01 - 1$, that is, diffusion and advection contributions are comparable. In the reservoirs Pe_r is smaller by a factor $R_r/R_p \sim 10 - 100$ and hence transport in the reservoirs can be diffusion dominated.

DNS of the model-H equations Eqs. (1) to (4) in the

bulk one-phase region up to 20 K from T_c, and with $R_p = 5$ nm, reveals three representative steady states with increasing Pe_p: (i) at small Pe_p, the adsorption in the pore, $\Gamma = \int_{pore}[\varphi - \varphi_0]\mathrm{d}^3\mathbf{r}$, remains close to its equilibrium value, (ii) at an intermediate Pe_p range, the adsorption in the pore is reduced to almost constant as a function of Pe_p, and (iii) at large Pe_p, the adsorption in the pore progressively decreases with Pe_p. In this Letter we focus on the first two cases.

In case (i), which is realized at $\mathrm{Pe}_p \lesssim 0.1$, the composition distribution in the pore changes very little compared to the classical equilibrium case [31], with $\varphi > \varphi_c$ throughout the pore as can be seen in Fig. 2(a). Most strikingly however, Fig. 2(a) also shows that the composition *outside* the pore is *not* equal to φ_c but is uniform and higher than φ_c in the outlet reservoir and non-uniform and smaller than φ_c in the inlet reservoir. This implies that there is a steady current of composition through the pore, which effectively acts as a selective membrane as it lets only a higher composition mixture to leave. To understand the origin of this intriguing effect we plot in Fig. 2(c) the time evolution of the profiles of the radially averaged composition, $\langle\varphi\rangle(z) = 2\pi\int\varphi(r,z)r\mathrm{d}r/A(z)$, where $A(z)$ is the cross section area. For visual clarity, we plot in Fig. 2(c) results for a longer pore with $L_p = 50$ but otherwise all the parameters are the same as in Fig. 2(a). Fig. 2(c) shows that shortly after the application of the pressure, a small excess composition is advected from the pore to the outlet reservoir; this excess composition diffuses quickly in the outlet, where the Péclet number is much smaller. The resulting depletion of composition in the pore is compensated by a predominantly diffusive current from the inlet reservoir, leading in turn to the small depletion in composition near the pore inlet. As time progresses, more of the excess composition in the pore is advected downstream and the outlet composition steadily increases, while at the same time the inlet reservoir is depleted. The inset of Fig. 2(c) shows the corresponding z-component of the composition current, $\boldsymbol{J}_z = 2\pi\int\left[\boldsymbol{j_a}_{,z} + \boldsymbol{j_d}_{,z}\right]r\mathrm{d}r$, revealing that the composition current from the inlet grows until it is able to compensate the current out of the pore. When this occurs the excess composition in the outlet eventually saturates at a constant steady state composition $\langle\varphi\rangle_{\mathrm{out}}$. The value of $\langle\varphi\rangle_{\mathrm{out}} \approx 0.06$ in Fig. 2(c) is a significant deviation from the critical composition, especially considering that in our weak adsorption model the average excess composition in the pore is only ≈ 0.1.

In short, adsorption in pores at small Pe_p allows to separate out the binary mixture component that is preferably adsorbed in the pore. Thus, relatively large nanopores can effectively act as a weakly selective membrane, by applying only a small pressure of $p < 1$ bar, with possibly an extremely low energy consumption in membrane processes [9]. What enables this extraordinary behaviour is the interplay between advection and diffusion that develops *inside* the pore at $\mathrm{Pe}_p \lesssim 0.1$. In this Pe_p regime, a diffusive flux, counteracting partially the advective flux, is able to develop in order to restore the energetically favorable equilibrium adsorption. However, at finite Pe_p there is always a residual advective flux and an excess composition in the outlet at steady state as a byproduct. The existence of a steady-state relies on the inlet reservoir being able to supply the constant current of excess composition, which in our model is guaranteed by constraining $\varphi = 0$ at $z = L$, with this constraint satisfied naturally for $L \to \infty$ or at least for a significant duration of time even when the reservoir can be depleted [31].

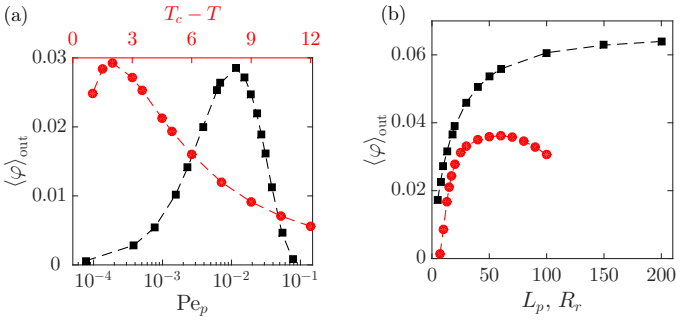

FIG. 3. (a) dependence of the outlet reservoir composition $\langle\varphi\rangle_{\mathrm{out}}$ on the pore Péclet number (squares, black abscissa) and deviation from the critical temperature (circles, red abscissa). (b) dependence of $\langle\varphi\rangle_{\mathrm{out}}$ on the pore volume and inlet reservoir volume. The pore volume changes linearly by varying L_p (squares) and keeping R_p fixed and the reservoir volume changes quadratically by varying R_r (circles) and keeping L fixed. In both panels, the basis parameter set is $T = T_c - 3$ K, $u_p = 0.05$ mm/s ($\mathrm{Pe}_p = 0.0077$), $L_p = 10$, $R_r = 20$ and $L = 10^3$, excluding the abscissa parameter. Lines are a guide to the eye.

At steady state, the diffusive current inside the pore is almost uniform (except near the pore mouths), and points in the $\hat{z}$ direction, opposite to the incoming flow [31]. This leads to a uniform body force in the same direction which is most significant near the pore walls where the local capillary number is small. This creates a back-flow near the wall, resulting in a far-from–parabolic velocity profile inside the pore. Since the volumetric flow rate is constant this implies two planes of zero velocity and an increase of the flow in the center. These features are visualized in Fig. 2(b), which shows v_z and streamlines corresponding to Fig. 2(a), and in Fig. 4(b), which shows the large deviation from Hagen–Poiseuille flow.

In Fig. 3 we show the effects of varying some of the free parameters of our system on the outlet reservoir composition $\langle\varphi\rangle_{\mathrm{out}}$. Fig. 3(a) verifies the small Pe_p regime (squares, black abscissa), showing that $\langle\varphi\rangle_{\mathrm{out}}$ increases with Pe_p as more material is advected out of the pore but then vanishes gradually beyond $\mathrm{Pe}_p \sim 0.1$ when axial diffusion can no longer maintain a steady current. Fig. 3(a)

also shows that a temperature that maximizes $\langle\varphi\rangle_{\rm out}$ exists (circles, red abscissa) because close to T_c $\mathrm{Pe}_p \propto D^{-1}$ becomes very large whereas far from T_c the adsorption in the pore is diminished. Note that $\langle\varphi\rangle_{\rm out}$ decreases slowly for large $T_c - T$ and is still significant up to 10 K from T_c. The effect of increasing L_p on $\langle\varphi\rangle_{\rm out}$ is plotted in Fig. 3(b) with R_p fixed (squares). For small L_p, $\langle\varphi\rangle_{\rm out}$ increases rapidly but then saturates when transport within the pore becomes the limiting factor, showing that above $L_p \sim 100$ gains in $\langle\varphi\rangle_{\rm out}$ are marginal. Changing R_r at fixed L (Fig. 3(b), circles), we find that an optimal value of R_r exists. Since we fix also Pe_p here, the reservoir Péclet number Pe_r decreases linearly with R_r. In the limit of a single long channel ($R_r \to 1$), $\mathrm{Pe}_r \to \mathrm{Pe}_p$ and advection in the outlet reservoir is dominant, leading to $\langle\varphi\rangle_{\rm out} \to 0$. When R_r becomes very large, $\mathrm{Pe}_r \to 0$, reducing the total current from the inlet which leads to a decrease in $\langle\varphi\rangle_{\rm out}$. The results in Fig. 3 should serve a guideline for the future design and optimization of membranes. We speculate that similar results would be obtained whenever a wetting film comparable in size to R_p exists, for example, when capillary condensation occurs.

Upon increasing the external pressure the near-equilibrium adsorption cannot be maintained in any cross section along the pore axis, and a new type of steady state, case (ii), is reached. In Fig. 4(a) we show a representative composition map for $\mathrm{Pe}_p = 0.77$, where we used the same parameters as in Fig. 2(a) but increased u_r. Here, the adsorption at the pore wall is still significant and not far from the equilibrium value. However, φ decays in the radial direction to a value that is smaller than φ_c at the pore center (which is not possible in equilibrium within our continuum description). In this steady state the critical composition flows uninterrupted from the inlet reservoir to the outlet as there is no net composition current through the system. Furthermore, our DNS show that both the axial diffusive and axial advective current in the pore vanish. Having $\boldsymbol{j_d}_{,z} = 0$ implies a uniform chemical potential in the pore and therefore no body-force on the fluid. Thus, the velocity profile has a simple parabolic shape (see Fig. 4(b)) and being unidirectional, $\boldsymbol{j_a}_{,z} = 0$ means there must be a region of $\varphi < \varphi_c$ for some r. Hence, the flow effectively shifts the chemical potential to a smaller value $\mu_{\rm eff} < 0$, which, since $\mu_{\rm eff}$ is constant, corresponds to an equilibrium adsorption for some $\varphi_0 < \varphi_c$.

An estimate of $\mu_{\rm eff}$ can be calculated within a standard approximation neglecting the φ^3 term in μ [39]. Ignoring small axial components inside the pore the composition profile is obtained from a simplified Eq. (2) which reads $\mu_{\rm eff} = -\epsilon(\varphi_{rr} + \varphi_r/r) + \alpha\varphi$. This equation is solved together with the BCs $\varphi_r(0) = 0$, $\varphi_r(1) = \gamma/\epsilon$ and the constraint $\boldsymbol{j_a}_{,z} = 2\pi \int_0^1 \left[-2\mathrm{Pe}_p(1-r^2)\varphi(r)\right] r dr = 0$, which determines $\mu_{\rm eff}$. The resulting composition profile is

$$\varphi(r) = \gamma/(\epsilon\zeta I_1(\zeta)) \times \left[I_0(r\zeta) - 8I_2(\zeta)/\zeta^2\right] \ , \qquad (5)$$

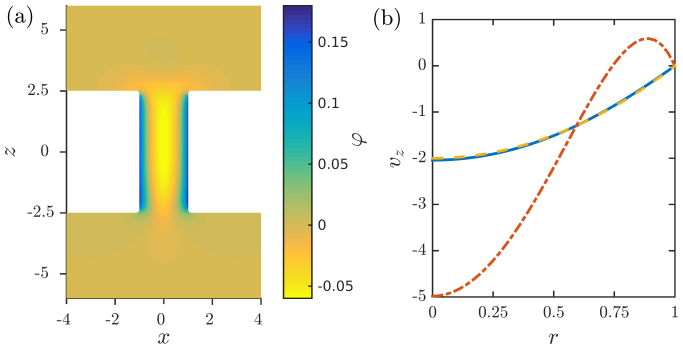

FIG. 4. (color online) (a) composition for case (ii) steady state. Parameters are the same as in Fig. 2 but with $u_p = 5$ mm/s ($\mathrm{Pe}_p = 0.77$). (b) velocity profiles $v_z(r)$ at the pore center ($z = 0$) for a single-component fluid ($v_z = -2(1-r^2)$, dashed line) and for case (i) in Fig. 2 and for case (ii) in this figure (dash-dot and solid lines, respectively)

where $\zeta = \sqrt{\alpha/\epsilon} = \sqrt{2}R_p/\xi$ and I_n are n-th order modified Bessel functions of the first kind. The first term in the brackets is the adsorption profile with no flow while the second term is the constant r-independent negative shift of φ due to the flow. Strikingly, this result is independent of Pe_p. Indeed, our DNS confirm that the composition profile in the pore is unchanged for the parameters of Fig. 2, in the range $0.5 \lesssim \mathrm{Pe}_p \lesssim 10$.

Our results imply that solutes that interact favorably with the $\varphi < 0$ phase will, for a wide range of applied pressures, be focused in the internal cylindrical region while being transported through the pore, and therefore, we speculate that the pore could exhibit anti-fouling behaviour [5], depending on the solute-wall interaction strength. The circular cross section for which $\varphi < 0$ is found at $r \approx 0.6R_p$ and this value is relatively insensitive to temperature. However, the affinity of solutes to the central region can be tuned externally via temperature. As $T \to T_c$, φ in the internal region becomes more negative.

Finally, when the pressure is even further increased, steady state case (iii) is gradually reached. The adsorption in the pore further decreases until only a thin adsorbed layer near the wall remains. The excess material initially advected out of the pore is expelled into a reservoir where Pe_r is much smaller and is therefore dispersed slowly downstream. The result [31] is a steady state composition distribution in the reservoir that can extend over a huge distance of $O(\mu\mathrm{m})$. This regime will be investigated in more detail in a future publication.

In conclusion, we predict that a tunable composition current can be pushed through a nanopore, and that the pore composition can be controlled reversibly by either temperature or pressure. The consequences of these phenomena on the transport of solutes through the pore is an intriguing possibility which we hope will motivate experimental work.

We acknowledge discussions with R. Evans and the anonymous referees for their useful comments. R.v.R acknowledges financial support of a Netherlands Organisation for Scientific Research (NWO) VICI grant funded by the Dutch Ministry of Education, Culture and Science (OCW). S.S acknowledges funding from the European Union's Horizon 2020 research and innovation programme under the Marie Skłodowska-Curie grant agreement No. 656327. This work is part of the D-ITP consortium, a program of the Netherlands Organisation for Scientific Research (NWO) funded by the Dutch Ministry of Education, Culture and Science (OCW). DNS in this work were performed using the COMSOL multiphysics software v5.1.

* S.Samin@uu.nl

[1] M. M. Pendergast and E. M. V. Hoek, Energy & Environmental Science **4**, 1946 (2011).
[2] M. R. Powell, L. Cleary, M. Davenport, K. J. Shea, and Z. S. Siwy, Nature Nanotechnology **6**, 798 (2011), 81.
[3] M. Carta, R. Malpass-Evans, M. Croad, Y. Rogan, J. C. Jansen, P. Bernardo, F. Bazzarelli, and N. B. McKeown, Science **339**, 303 (2013).
[4] L. Wang, Y. Zhao, Y. Tian, and L. Jiang, Angew. Chem. Int. Ed. **54**, 14732 (2015).
[5] X. Hou, Y. Hu, A. Grinthal, M. Khan, and J. Aizenberg, Nature **519**, 70 (2015), 10.
[6] M. Adebajo, R. Frost, J. Kloprogge, O. Carmody, and S. Kokot, Journal of Porous Materials **10**, 159 (2003).
[7] P. J. M. Monteiro, C. H. Rycroft, and G. I. Barenblatt, Proc. Nat. Acad. Sci. USA **109**, 20309 (2012).
[8] T. Lee, L. Bocquet, and B. Coasne, Nat Comms **7**, 11890 (2016).
[9] P. Marchetti, M. F. Jimenez Solomon, G. Szekely, and A. G. Livingston, Chem. Rev. **114**, 1073510806 (2014).
[10] M. Amirilargani, M. Sadrzadeh, E. Sudhlter, and L. de Smet, Chem. Eng. J. **289**, 562582 (2016).
[11] S. Gravelle, H. Yoshida, L. Joly, C. Ybert, and L. Bocquet, J. Chem. Phys. **145**, 124708 (2016).
[12] A. Onuki, J. Phys.: Condens. Matter **9**, 6119 (1997).
[13] H. Tanaka, J. Phys.: Condens. Matter **13**, 4637 (2001).
[14] K. Binder, S. Puri, S. K. Das, and J. Horbach, Journal of Statistical Physics **138**, 51 (2010).
[15] L. Bocquet and E. Charlaix, Chem. Soc. Rev. **39**, 1073 (2010).
[16] M. Rauscher and S. Dietrich, Annu. Rev. Mater. Res. **38**, 143 (2008).
[17] D. Lohse and X. Zhang, Rev. Mod. Phys. **87**, 981 (2015).
[18] P. Huber, J. Phys.: Condens. Matter **27**, 103102 (2015).
[19] O. Vincent, A. Szenicer, and A. D. Stroock, Soft Matter **12**, 6656 (2016).
[20] J. M. Oh, T. Faez, S. de Beer, and F. Mugele, Microfluid Nanofluid **9**, 123 (2009).
[21] F. H. J. van der Heyden, D. Stein, and C. Dekker, Phys. Rev. Lett. **95** (2005), 10.1103/physrevlett.95.116104.
[22] F. H. J. van der Heyden, D. Stein, K. Besteman, S. G. Lemay, and C. Dekker, Phys. Rev. Lett. **96** (2006), 10.1103/physrevlett.96.224502.
[23] D. Lis, E. H. G. Backus, J. Hunger, S. H. Parekh, and M. Bonn, Science **344**, 11381142 (2014).
[24] R. Khare, M. D. Graham, and J. J. de Pablo, Phys. Rev. Lett. **96** (2006), 10.1103/physrevlett.96.224505.
[25] L. Graetz, Annalen der Physik **254**, 79 (1882).
[26] W. M. Deen, *Analysis of Transport Phenomena*, 2nd ed., Topics in Chemical Engineering (Oxford University Press, 2011).
[27] M. E. Fisher and P. G. de Gennes, C. R. Seances Acad. Sci. Ser. B **287**, 207 (1978).
[28] U. M. B. Marconi, Phys. Rev. A **38**, 6267 (1988).
[29] A. Maciołek, R. Evans, and N. B. Wilding, J. Chem. Phys. **119**, 8663 (2003).
[30] D. M. Anderson, G. B. McFadden, and A. A. Wheeler, Annu. Rev. Fluid Mech. **30**, 139 (1998).
[31] For details see the supplemental material. ().
[32] S. Safran, *Statistical Thermodynamics of Surfaces, Interfaces, and Membranes* (Westview Press, New York, 1994).
[33] Our results remain qualitatively the same and quantitatively similar when a slip velocity up to $0.5u_p$ is prescribed at the pore wall. ().
[34] This BC implies that the dynamics of the surface order parameter is much faster than that of φ [14]. ().
[35] J.-H. J. Cho and B. M. Law, Phys. Rev. Lett. **86**, 2070 (2001).
[36] C. A. Grattoni, R. A. Dawe, C. Y. Seah, and J. D. Gray, J. Chem. Eng. Data **38**, 516 (1993).
[37] K. Kawasaki, Annals of Physics **61**, 1 (1970).
[38] It should be noted that the explicit use of D in Eq. (1) implies that the Debora number, $\mathrm{De} = S\xi^2/D$, where S is a characteristic shear rate, is small throughout the system (see [12] for a detailed discussion). $\mathrm{De} \ll 1$ holds for almost all of our calculations, except close to T_c and for large Pe_p, where $\mathrm{De} \gtrapprox 1$ near the pore wall. ().
[39] A. Onuki, *Phase transition dynamics* (Cambridge University Press, 2004).